The Journal of Neuroscience

http://jneurosci.msubmit.net

JN-RM-0005-16R3

# A critical role for astrocytes in hypercapnic vasodilation in brain

Brian MacVicar, University of British Columbia
Clare Howarth, The University of Sheffield
Brad Sutherland, University of Oxford
Hyun Choi, University of British Columbia
Chris Martin, University of Sheffield
Barbara Lind, University of Copenhagen
Lila Khennouf, University of Copenhagen
Jeffrey LeDue, University of British Columbia
Janelle Pakan, University of Edinburgh
Rebecca Ko, University of British Columbia
Graham Ellis-Davies, Mount Sinai School of Medicine
Martin Lauritzen, Panum Institute
Nicola Sibson, University of Oxford
Alastair M. Buchan, University of Oxford

Commercial Interest:

# A critical role for astrocytes in hypercapnic vasodilation in brain

Abbreviated title: Glutathione-dependent cerebral blood flow control

C. Howarth[1,2,4,*], B.A. Sutherland[3,8*], H.B. Choi[1], C. Martin[2,4], B.L. Lind[5], L. Khennouf[5], J.M. LeDue[1], J.M.P. Pakan[1], R.W. Ko[1], G.C.R. Ellis-Davies[6], M.J. Lauritzen[5,7], N.R. Sibson[2], A.M. Buchan[3] & B.A. MacVicar[1]

[1]Djavad Mowafaghian Centre for Brain Health, University of British Columbia, Vancouver, V6T 1Z3, Canada [2]Cancer Research UK and Medical Research Council Oxford Institute for Radiation Oncology, Dept. of Oncology, University of Oxford, Oxford, OX3 7DQ, UK [3]Acute Stroke Programme, Radcliffe Dept. of Medicine, University of Oxford, Oxford, OX3 9DU, UK [4]Department of Psychology, University of Sheffield, Sheffield, S10 2TP, UK [5]Department of Neuroscience and Pharmacology and Center for Healthy Aging, University of Copenhagen, DK-2200 Copenhagen N, Denmark [6]Department of Neuroscience, Mount. Sinai School of Medicine, New York, NY 10028, USA [7]Department of Clinical Neurophysiology, Rigshospitalet, DK-2600 Glostrup, Denmark [8]Present address: School of Medicine, University of Tasmania, Hobart, Australia

[*] These authors contributed equally to this work.

Corresponding author: Brian MacVicar (Djavad Mowafaghian Centre for Brain Health, 2211 Wesbrook Mall, University of British Columbia, Vancouver, V6T 1Z3, Canada, +1 604 822 7797, bmacvicar@brain.ubc.ca) or Alastair Buchan (Acute Stroke Programme, Radcliffe Dept. of Medicine, University of Oxford, Oxford, OX3 9DU, UK, +44 1865 220 346, alastair.buchan@medsci.ox.ac.uk).

Number of pages: 36

Number of figures: 7 Number of tables: 2

Number of words: Abstract: 227 Introduction: 509 Discussion: 1191

Conflict of Interest: The authors declare no competing financial interests.

Acknowledgements: This work was funded by a Sir Henry Wellcome Post-Doctoral Fellowship (CH), a Government of Canada Post-Doctoral Research Fellowship (CH), a Michael Smith Foundation for Health Research Post-Doctoral Fellowship (CH), a Natural Sciences and Engineering Research Council (NSERC) Post-Doctoral Fellowship (JMPP), a CIHR Doctoral Studentship (RWK), a Canada Research Chair in Neuroscience (BAM), Canadian Institutes of Health Research (CIHR) operating grants (#148397, #8545, #115121 and TCE-117869 in the framework of the ERA-NET NEURON) (BAM), Fondation Leducq (BAM, AMB, MJL), Human Frontiers Science Program (BAM, GED), NIH (GM053395 and NS069720) (GED), Heart and Stroke Foundation (BAM, HBC), The Wellcome Trust (CM), Royal Society University Research Fellowship (CM), Cancer Research UK (C5255/A12678) (NRS), The Henry Smith Charity (AMB), NORDEA Foundation for the Center for Healthy Aging (MJL), the Lundbeck Foundation (MJL), the NOVO-Nordisk Foundation (MJL) and the Danish Medical Research Council (MJL). We thank David Attwell for discussions regarding this work.

**Abstract**

Cerebral blood flow (CBF) is controlled by arterial blood pressure, arterial $CO_2$, arterial $O_2$, and brain activity and is largely constant in the awake state. Although small changes in arterial $CO_2$ are particularly potent to change CBF (1 mmHg variation in arterial $CO_2$ changes CBF by 3-4%), the coupling mechanism is incompletely understood. We tested the hypothesis that astrocytic prostaglandin $E_2$ ($PgE_2$) plays a key role for cerebrovascular $CO_2$ reactivity and that preserved synthesis of glutathione is essential for the full development of this response.

We combined two-photon imaging microscopy in brain slices with *in vivo* work in rats and C57Bl/6J mice to examine the hemodynamic responses to $CO_2$ and somatosensory stimulation before and after inhibition of astrocytic glutathione and $PgE_2$ synthesis. We **demonstrate that hypercapnia (increased $CO_2$) evokes an increase in astrocyte $[Ca^{2+}]_i$ and stimulates COX-1 activity.** The enzyme downstream of COX-1 that synthesizes $PgE_2$ (microsomal prostaglandin E synthase-1) depends critically for its vasodilator activity on the level of glutathione in the brain. **We show that w**hen glutathione levels are reduced, astrocyte **calcium-evoked** release of $PgE_2$ is decreased and vasodilation triggered by astrocyte $[Ca^{2+}]_i$ *in vitro* and by hypercapnia *in vivo* is inhibited.

Astrocyte synthetic pathways, dependent on glutathione, are involved in cerebrovascular reactivity to $CO_2$. Reductions in glutathione levels in ageing, stroke or schizophrenia could lead to dysfunctional regulation of CBF **and subsequent neuronal damage.**

**Keywords:** astrocyte, cerebral blood flow, calcium, glutathione, hypercapnia

## Significance statement

Neuronal activity leads to the generation of $CO_2$, which has previously been shown to evoke cerebral blood flow (CBF) increases via the release of the vasodilator $PgE_2$. We demonstrate that hypercapnia (increased $CO_2$) evokes increases in astrocyte calcium signaling which in turn stimulates COX-1 activity and generates downstream $PgE_2$ production. We demonstrate that astrocyte calcium-evoked production of the vasodilator, $PgE_2$, is critically dependent on brain levels of the antioxidant, glutathione. These data suggest a novel role for astrocytes in the regulation of $CO_2$-evoked CBF responses. Furthermore, these results suggest that depleted glutathione levels, which occur in ageing and stroke, will give rise to dysfunctional cerebral blood flow regulation and may result in subsequent neuronal damage.

## Introduction

Astrocyte $[Ca^{2+}]_i$ transients have been shown to directly alter diameters of cerebral arterioles in experiments using either direct astrocyte stimulation or calcium uncaging in astrocytes of juvenile (Zonta et al., 2003; Mulligan and MacVicar, 2004; Gordon et al., 2008), or adult animals (Takano et al., 2006). However, several labs have published contradictory evidence on whether, in adult animals, astrocyte $[Ca^{2+}]_i$ signaling is evoked by synaptic activity leading to neurovascular coupling (Zonta et al., 2003; Petzold et al., 2008; Schulz et al., 2012; Lind et al., 2013; Otsu et al., 2015) or not (Nizar et al., 2013; Takata et al., 2013; Bonder and McCarthy, 2014). More recently, astrocyte $[Ca^{2+}]_i$ was shown to modify basal arteriole tone in adult animals (Rosenegger et al., 2015). Therefore, it is still poorly understood when, how, and under what conditions, astrocyte $[Ca^{2+}]_i$ signaling contributes to the regulation of cerebral blood flow (CBF).

In this work, we investigated the mechanisms underlying CBF responses to increased blood $CO_2$ concentrations (hypercapnia) and the potential contribution of astrocytes to those CBF responses. Arterial $CO_2$ has a potent effect on CBF, with a 1 mmHg variation eliciting a 3-4% CBF change (Hauge et al., 1980). However, the mechanism coupling a change in $CO_2$ to a change in CBF is incompletely understood. There are parallels between the vasoactive signals generated by astrocytes and those underlying hypercapnia-evoked CBF responses. Astrocytes have been shown to directly modify arteriole diameter when their intracellular $[Ca^{2+}]_i$ increases, activating $PLA_2$ (He et al., 2012) and thereby generating arachidonic acid (AA) and several vasoactive metabolites including $PgE_2$, which causes vasodilation (Zonta et al., 2003; Takano et al., 2006; Gordon et al., 2008; Attwell et al., 2010). In addition to their roles in neurovascular coupling, both $PgE_2$ (Wagerle and Mishra, 1988; Wagerle and Degiulio, 1994) and cyclooxygenase-1 (COX-1) activity (Niwa et al., 2001) are involved in increasing CBF during hypercapnia. We examined the potential link between astrocytes and increased CBF during hypercapnia because astrocytes express the enzymes that are involved in synthesizing $PgE_2$ from AA during hypercapnia induced CBF changes (Niwa et al., 2001). For example, mRNA for both COX-1 and microsomal prostaglandin E synthase-1 (mPgES-1) are reported in transcriptome studies to be highly expressed in astrocytes but not neurons (e.g. ptgs1, also known as COX-1, is 15-fold higher in astrocytes than in neurons (Cahoy et al., 2008; Zhang et al., 2014)). Astrocytes are immunoreactive for both the enzyme proteins COX-1 (Takano et al., 2006; Gordon et al., 2008) and mPgES-1 (Figure 3A and Tachikawa et al., 2012). mPgES-1, the form of prostaglandin E synthase expressed in astrocytes, requires the co-factor glutathione (GSH) (Jakobsson et al., 1999; Murakami et al., 2000) that is present in high levels in astrocytes (Figure 3B and Sun et al., 2006; Bragin et al., 2010; Robillard et al., 2011). We investigated whether hypercapnia can evoke an increase in astrocyte $[Ca^{2+}]_i$ *in vivo* and, if so, whether this results in activation of a $PgE_2$-mediated

vasodilation. In doing so, we demonstrate a novel, GSH dependent mechanism of CBF regulation which involves astrocytes and the GSH-sensitive release of $PgE_2$.

## Materials and Methods

### *Slice preparation*

400μm hippocampal-neocortical slices were prepared from male and female juvenile (postnatal age 16-21 days) Sprague-Dawley rats. Treatment of animals was approved by the University of British Columbia Animal Care and Use Committee. As previously described (Gordon et al., 2008), rats were anaesthetized with halothane, decapitated and the brains removed into ice-cold slicing solution containing (in mM): KCl, 2.5; $NaHCO_3$, 26; $CaCl_2$, 0.5; $MgSO_4$, 10; $NaH_2PO_4$, 1.25; glucose, 10; sucrose, 230; saturated with 95% $O_2$/5% $CO_2$. 400 μm transverse hemi-sections were incubated at 32-34°C in aCSF containing (in mM): NaCl, 126; KCl, 2.5; $NaHCO_3$, 26; $CaCl_2$, 2.0; $MgCl_2$, 2; $NaH_2PO_4$, 1.25; glucose, 10; saturated with 95% $O_2$/5% $CO_2$ for 60 min. For experiments, slices were at 22–24°C, aCSF was saturated with 20% $O_2$/5% $CO_2$, balanced $N_2$ and perfused at ~2 ml/min. Healthy slices can be maintained in 20% $O_2$, which provides a $pO_2$ at the low end of the physiological range (Gordon et al., 2008). Astrocytes were loaded with the caged $IP_3$ compound, NV-$IP_3$/AM (5μg/ml) and/or the $Ca^{2+}$ indicator rhod-2/AM (10μM, Invitrogen) as previously described (Mulligan and MacVicar, 2004; Gordon et al., 2008). Slices were loaded with monochlorobimane (MCB, Fluka) in the dark at room temperature for 30 minutes as previously described (Robillard et al., 2011).

### *Two-photon imaging and uncaging in acute brain slices*

A two-photon laser-scanning microscope (Zeiss LSM510-Axioskop-2 fitted with a 40X-W/1.0 numerical aperture objective lens) coupled to a Chameleon ultra II Ti:sapphire laser (~140-fs pulses 80 MHz, Coherent) provided excitation of rhod-2 and was used to uncage $IP_3$. Images were acquired 50-100μm below the slice surface. Rhod-2 fluorescence imaging and two-photon uncaging was performed using laser settings and emission filters as previously described (Gordon et al., 2008). MCB was excited at 780nm and detected with a PMT at 512-562nm as previously described (Robillard et al., 2011). Arterioles (defined as vessels with diameter >10μm, surrounded by a visible layer of smooth muscle cells) were imaged by acquiring the transmitted laser light and using IR-DIC optics.

***Glutathione and $PgE_2$ measurements***

Protocols in suppliers' instructions were followed for the $PgE_2$ ELISA and glutathione assays. When measuring $PgE_2$ release from acute brain slices, tetrodotoxin (1μM, Alamone Labs) was added to dampen neuronal activation. $PgE_2$ release from acute brain slices was measured using a Specific Parameter $PgE_2$ ELISA kit (R&D systems, Minneapolis, MN, USA). Measurements of tissue glutathione levels were made using a specific total glutathione assay kit from either BioVision (Milpitas, CA, USA) or Assay Designs (Ann Arbor, MI, USA).

***Immunohistochemistry***

Rats were anesthetized with halothane, given an intraperitoneal injection of urethane (0.5ml of 30% urethane per 50g body weight) and perfused with saline (0.9% NaCl in 0.1M phosphate buffer) followed by 4% paraformaldehyde (PFA; in 0.1M phosphate buffered saline (PBS)). The brain was extracted, post-fixed (10% sucrose in 4% PFA) overnight and cryoprotected (30% sucrose in PBS) overnight. Using a cryostat, 40μm serial sections in the horizontal plane were collected throughout the brain. Free-floating sections were blocked

with 10% normal goat serum (NGS; Jackson Immunoresearch Laboratories, West Grove, PA) and 0.4% TritonX-100 in PBS for 1 hour and incubated in PBS containing 0.1% TritonX-100 and primary antibodies against $PgE_2$ synthase (anti-mPgES-1 (Olajide et al., 2014; Tuure et al., 2014), Agrisera, [Catalogue number: AS03 031], 1:200) as well as an astrocyte phenotypic marker (anti-GFAP (Lathia et al., 2008), Sigma, [Catalogue number: G3893, Clone number: G-A-5], 1:500) overnight at 4°C. Tissue was rinsed and incubated in AlexaFluor 488 goat anti-mouse and AlexaFluor 546 goat anti-rabbit secondary antibodies (Molecular Probes: diluted 1:500 in PBS, 2.5% NGS and 0.4% TritonX-100) for 1.5 hours at room temperature. The tissue was rinsed, mounted onto slides and coverslipped using Fluorsave mounting medium (Calbiochem). Images were acquired with an Olympus Fluoview FV1000 confocal microscope.

***Drugs***

tACPD, clonidine, norepinephrine (Sigma) and $PgE_2$ (Cayman Chemicals) were bath applied for 5–10min. SC560 (Sigma) was pre-incubated for 30 minutes (Blanco et al., 2008) followed by bath application and BSO (Sigma) was preincubated for 2.5 hours (Sun et al., 2006) followed by bath application throughout the experiment. NV-$IP_3$/AM was synthesized by G. Ellis-Davies.

***Animals - In vivo blood flow measurements in rats***

All procedures were approved by the University of Oxford Ethical Review Committee and complied with the requirements of the Animals (Scientific Procedures) Act, 1986, UK. Animals were housed in an animal housing facility in a 12hr alternating light:dark cycle with *ad libitum* access to food and water. Male Wistar rats were used (256 - 367g).

***Intracerebral injection***

For surgical procedures, rats were anaesthetised with 4% isoflurane and maintained at 1.5-2% isoflurane in 30% $O_2$ and 70% $N_2O$. Each rat was placed in a stereotaxic frame and the skull exposed. A burr hole was drilled at 1mm caudal and 4.2mm lateral to bregma, and the dura mater was finely dissected away to expose the cortex. 20µl of 80mg/mL BSO (Pileblad and Magnusson, 1989) or 0.9% saline was infused by a microinfusion pump at a rate of 2µl/min into the right whisker barrel cortex at a depth of 2.3mm from the brain's surface. This dose of BSO has previously been shown to adequately reduce GSH within 24 hours of administration (Pileblad and Magnusson, 1989), and we showed that BSO administered in this way could decrease GSH levels in the ipsilateral cortex by 45%, 24 hours post-injection (Figure 5C), and in the ipsilateral striatum by 31% (GSH (mM) measured in saline-treated: 0.61±0.03mM, BSO-treated: 0.42±0.08mM, p = 0.045, n = 7 per group, values expressed as mean±s.e.m.). After the infusion, bone wax was placed over the burr hole and the wound was closed with 3-0 sutures. Animals recovered for 24 hours prior to assessment of GSH levels (n = 7 per group) or evoked blood flow responses (n = 6-10 per group).

***Whisker pad stimulation and hypercapnia: In vivo blood flow measurements***

24 hours post-BSO/saline treatment, animals had their left femoral artery cannulated for blood gas measurement and were tracheotomised and ventilated with 1.25% isoflurane in 30% $O_2$ and 70% $N_2$. A laser Doppler probe (Perimed, Järfälla, Sweden) to monitor relative cerebral blood flow (CBF) was placed over the right whisker barrel cortex (where the intracerebral injection was made) and bipolar stimulating electrodes were placed in the left whisker pad. For some experiments, a local field potential (LFP) electrode for neuronal activity was also placed on the exposed cortex to monitor neuronal activity. All animals had a steady state blood gas (see Table 1) prior to beginning experiments.

205 An electrical stimulus (10Hz, 16s duration, 1.6mA, 0.3ms pulsewidth, 60s interstimulation
206 interval) to evoke a blood flow response in the right whisker barrel cortex was carried out for
207 10 trials per animal. Following this, animals were exposed to 10% $CO_2$ for 30s at 3 min
208 intervals repeated four-five times to induce hypercapnic blood flow responses. Animals were
209 euthanized and the cortex dissected for measurement of GSH levels.

210 For SC560 experiments, naïve rats were anaesthetized with isoflurane. Anaesthesia was
211 induced with 4% isoflurane and maintained during surgery with 2% isoflurane. During
212 stimulation, anaesthesia was maintained with 1.25% isoflurane. Isoflurane was carried in
213 30% $O_2$ and 70% $N_2$. Rats had their left femoral artery and vein cannulated, and were also
214 tracheotomised and ventilated. A laser speckle camera (Moor Instruments, Axminster, UK)
215 was used to monitor relative CBF over a thin skull window over the right whisker barrel
216 cortex while an LFP electrode for neuronal activity was inserted through a burr hole. Bipolar
217 stimulating electrodes were placed in the left whisker pad. Animals had a steady state blood
218 gas prior to and after drug administration (see Table 2). An electrical stimulus (10Hz, 16s
219 duration, 1.6mA, 0.3ms pulsewidth, 60s interstimulation interval) to evoke a blood flow
220 response in the right whisker barrel cortex was carried out for 10 trials per animal. Following
221 this, animals were exposed to 10% $CO_2$ for 30s at 3 min intervals repeated four times to
222 induce a hypercapnic blood flow response. Animals were then administered 5mg/kg SC560
223 or 10% DMSO (vehicle) intravenously. SC560 is a highly lipophilic COX-1 inhibitor and
224 distributes widely into tissues (Teng et al., 2003), and this dose was chosen for maximal
225 target efficiency (Zhang et al., 2003). After 20 minutes, the effect of COX-1 inhibition on the
226 evoked CBF responses to whisker stimulation and hypercapnia were measured.

227 ***Animals – In vivo calcium imaging***

For *in vivo* experiments, all procedures involving animals were approved by the Danish National Ethics Committee according to the guidelines set forth in the European Council's Convention for the Protection of Vertebrate Animals used for Experimental and Other Scientific Purposes. 8-10 week old male C57Bl/6J mice were used.

***In vivo calcium imaging***

For experiments involving mice, anaesthesia was induced with bolus injections of the α2-adrenergic receptor agonist xylazine (10mg/kg i.p.) and the NMDA-receptor antagonist ketamine (60mg/kg i.p.). Anaesthesia was maintained during surgery with supplemental doses of ketamine (30 mg/kg/20 min i.p.). Upon completion of all surgical procedures, anesthesia was switched to continuous infusion with α-chloralose (50 mg/kg/h i.v.).

Calcium activity during hypercapnia was measured *in vivo* in eight C57Bl/6J mice. A craniotomy over the somatosensory cortex was covered with agarose and partly sealed with a glass cover slip. Oregon Green Bapta-1/AM (OGB; Invitrogen, Molecular Probes) was dissolved in DMSO and Pluronic F-127 (10%, BASF Global), and diluted in aCSF to yield a final dye concentration of 0.8 mM. It was mixed with the astrocyte marker sulforhodamine 101 (SR101; Sigma-Aldrich, 100 μM (Nimmerjahn et al., 2004)), and was pressure injected (4–6 psi, 4s) into the somatosensory cortex through a micropipette at a depth of 100–150μm below the cortical surface. $Ca^{2+}$ imaging was performed using a commercial two-photon microscope (SP5 multiphoton/confocal Laser Scanning Microscope; Leica, Germany), and a Mai Tai HP Ti:sapphire laser (Millennia Pro, Spectra Physics, Sweden) with a 20× 1.0 NA-water-immersion objective (Leica, Germany). The excitation wavelength was 820 nm. The emitted light was filtered to retain both red and green light using a TRITC/FITC filter.

The hypercapnia challenge was presented as follows: Following 1 min baseline recording, 10% $CO_2$ in air was applied for 30s and imaging continued for subsequent 4 minutes. 5 trials were performed with 3 minutes between trials. For each animal, a second field of view was selected and the hypercapnia challenge repeated. Blood gases were taken after each experiment and all mice had $pCO_2$ in the range 30-40mmHg and $pO_2$ in the range 95-130mmHg.

***Data collection, analysis and statistics***

*In vitro data:* An image (512×512 pixels) was collected in 7.86-12.68s, using 8-line averaging. Measurements of lumen diameter and $Ca^{2+}$ changes were performed offline with Zeiss LSM (version 3.2) software and ImageJ (NIH). As previously described (Gordon et al., 2008), fluorescence signals were defined as $F/F_0$ (%) = $[(F_1\text{-}B_1)/(F_0\text{-}B_0)]100$ where $F_1$ and $F_0$ are fluorescence at a given time and the mean fluorescence during the control period, respectively. $B_1$ and $B_0$ are the corresponding background fluorescence signals, taken from the neuropil. Pseudo-colour images show absolute changes in fluorescence (ImageJ, 16-colour linear Lut). Experimental values are mean±s.e.m.; *n* is the number of experiments conducted or, for calcium changes, number of astrocytes analysed. Either a two-tailed Student's *t*-test or a one-way ANOVA with a Newman–Keuls post-hoc test for comparison between multiple groups was used and $p<0.05$ was considered statistically significant. As these were novel experiments, the effect size was unknown prior to experiment. Therefore, sample size estimates were based on our previous experience. Experiments were alternately performed under control or treatment conditions with slices chosen at random for each experiment. Data were excluded from analysis if any of the following occurred during imaging: unstable baseline vessel diameters or astrocyte calcium levels, or movement leading

to significant focus changes during the experiment. In order to perform statistical analysis, data were assumed to be normally distributed.

*In vivo data:* All laser Doppler and local field potential (LFP) data were collected in Spike 2 software while laser speckle data was collected using Moor FLPI software. Quantification of CBF changes and electrophysiology were performed in MATLAB (version 7.12). To obtain the region of interest (ROI) for calculation of CBF changes using laser speckle imaging, a principal components analysis was used to identify the focal point of the change in response to stimulation. The same region of interest was used within each animal's data. Experimental values are the mean±s.e.m. and $n$ is the number of animals. In order to perform statistical analysis, data were assumed to be normally distributed. An F-test was used to compare variances of groups being statistically compared. For CBF data, a one-tailed t-test with Welch's correction (as groups had significantly different variances) was used to compare means between groups. A two-tailed t-test was used to compare means of groups for both GSH analysis (Figure 5C) and electrophysiology data in response to whisker pad stimulation (Welch-corrected for SC560 experiment, Figure 6C). For electrophysiology data collected during hypercapnia challenge experiments, a two-way ANOVA with Bonferroni correction for multiple comparisons was used to compare means between groups. $p < 0.05$ was considered statistically significant. For experiments involving rats, due to effect sizes being unknown prior to experiment, sample size estimates were based on previously published sample sizes (for example, Niwa et al., (2001)). Assignment of animals was alternated between treatment and control groups and neither experiments nor analysis were blinded. Three animals were excluded from all data analysis (1 for SC560 and 2 for BSO) due to technical problems with experimental equipment.

For *in vivo* calcium imaging, frame size was 256 × 256 pixels (189-207 ms/frame) during recordings. The $Ca^{2+}$ changes were evaluated as the average change in fluorescence relative to baseline levels in ROIs. The ROIs were placed based on morphology over neuronal or astrocytic soma, or neuropil. Due to movement of astrocytes during hypercapnia, within or out of focus, ROIs were evaluated based on the level of SR101 loading in the red channel. If a significant change occurred, the ROI was disregarded in all following assessments. An increase in fluorescence within an ROI was classified as a calcium response if the mean fluorescence value **within the period of hypercapnia** was above two standard deviations of baseline activity. The delay of the $Ca^{2+}$ response was found by subtracting the signal onset time from the time hypercapnia was introduced to the animal. To estimate response start and termination time a fit was made to the data and the first and second order derivatives were calculated. The response onset time was found by taking the maximum peak of the second order derivative of the fitted data. The duration of the $Ca^{2+}$ response was then found by subtracting the response onset time from the response termination time. The response termination time was defined as the timepoint when the fitted data went below mean baseline $Ca^{2+}$ levels or the recording ended. Experimental values are expressed as mean±s.e.m. A paired t-test was used for the calcium imaging data, each animal served as its own control. $p < 0.05$ was accepted as statistically significant. For experiments involving mice, as there have been no previous studies reporting astroglial calcium changes during hypercapnia it was impossible to estimate an expected value for change in fluorescence or its standard deviation. Hence, no sample size calculation could be performed. However, we expected similar calcium changes to those which we observe for low frequency whisker stimulation and so sample sizes were based on our previous experiments (6-8 mice). Calcium signals obtained during hypercapnia exceeded an SNR of 4:1 and hypercapnia-induced calcium responses were recorded in every animal tested. As all mice were subjected to hypercapnia, there was

no randomization method used. Control measurements of calcium activity (i.e. activity without application of hypercapnia) were taken at random time points during the experiment. Analysis of calcium changes was not blinded, assessment of these changes was based on a MatLab program which analyzes the image sequences in an unbiased manner, rather than by visual inspection.

## Results

### Increased $CO_2$ evokes $[Ca^{2+}]_i$ responses in astrocytes *in vivo*

Elevation of tissue $CO_2$ concentration, which can be caused by neuronal metabolism, is known to dilate cerebral blood vessels in a process dependent on $PgE_2$ (Wagerle and Mishra, 1988; Wagerle and Degiulio, 1994) formation via COX-1 activity (Niwa et al., 2001). However the cells that both are responsible for sensing $CO_2$ and that also express the enzymes for synthesizing $PgE_2$ (COX-1 and Prostaglandin E synthase, PgES) have not been resolved. Astrocytes can produce $PgE_2$ but it is unknown if astrocytes generate $[Ca^{2+}]_i$ signals in response to $CO_2$. Therefore we tested whether an increase in inspired $CO_2$ (hypercapnia) *in vivo* evokes astrocyte $[Ca^{2+}]_i$ when it also triggers CBF increases.

Two photon laser scanning microscopy (2PLSM) *in vivo* was used to examine the simultaneous responses of both neurons and astrocytes to hypercapnia in the intact brain as a first step to investigate which cell type might be the primary sensor of $CO_2$ (Figure 1). Remarkably we found consistent and significant increases in $[Ca^{2+}]_i$ in the soma **and endfeet** of astrocytes in cortical layers II/III of mouse (Figure 1) during the period of hypercapnia. The dramatic increases that we observed in astrocytes were **of** significantly **higher amplitude** (Figure. 1A-C, $p<0.01$) than increases in $[Ca^{2+}]_i$ **observed** in neuronal soma

during the period of hypercapnia. The number of astrocytes with $[Ca^{2+}]_i$ responses was also much greater in hypercapnia compared to **the number showing spontaneous calcium activity** (control time period: Figure 1D, $p<0.01$). **Although neurons could display increased $[Ca^{2+}]_i$ during hypercapnia, with onset times within seconds (Figure 1B,C,E), there was no significant difference in the number of neurons with $[Ca^{2+}]_i$ responses during hypercapnia compared to the number showing spontaneous calcium activity (control time period: Figure 1D).** Measurements taken in the neuropil where there were no defined cell bodies and it is difficult to separate signals in fine astrocyte processes from neuronal processes did not show correlated changes in $[Ca^{2+}]_i$ signals during hypercapnia (Figure 1D). The astrocyte $[Ca^{2+}]_i$ responses (Figure 1B,E,F) **appear to occur within a similar timescale as** the increased CBF evoked by hypercapnia (as measured by laser speckle contrast imaging and laser Doppler flowmetry (LDF) in rat, Figure 5A and 5D, respectively). During hypercapnia, an increased number of astrocyte soma (Figure 1D) displayed increased $[Ca^{2+}]_i$ with onsets within seconds (Figure 1B,E) and variable durations of tens of seconds (Figure 1B,F). **While** there were no differences between the three groups (astrocyte soma, neuronal soma and neuropil) with regards to **the** delay of the hypercapnia-induced $Ca^{2+}$ responses (Average $Ca^{2+}$ response delay (Figure 1E): neuron soma = **12.14 ± 1.19s (n=33), neuropil = 12.83 ± 4.18s (n=3) and astrocyte soma = 14.57 ± 1.55s (n=47)**), **the a**verage $Ca^{2+}$ response duration (Figure 1F) **was found to be significantly longer in astrocytes than in neurons**: **neuron soma = 119.41 ± 8.82s (n=33), astrocyte soma = 155.47 ± 8.32s (n=47), $p<0.05$, ANOVA).**

### Astrocytic $[Ca^{2+}]_i$ signals evoke subsequent GSH-dependent $PgE_2$ release

Having demonstrated *in vivo* that hypercapnia evokes an increase in astrocyte $[Ca^{2+}]_i$, we then used a combination of 2PLSM and $PgE_2$ measurements using ELISA in acute brain

368 slices to determine the mechanistic links between astrocyte $[Ca^{2+}]_i$ responses and CBF
369 regulation. **Using a biochemical model, we investigated the role of GSH in the generation**
370 **of $PgE_2$.**

371 Unlike in the *in vivo* situation, it is difficult to reliably evoke astrocyte $[Ca^{2+}]_i$ signals
372 and vasodilations by applying $CO_2$ to acute brain slices. **Thus, we needed an alternative**
373 **method of elevating astrocyte $[Ca^{2+}]_i$ in acute brain slices. Although the adult mouse**
374 **(Sun et al., 2013) and rat (Duffy and MacVicar, 1995) have been shown to not express**
375 **functional mGluR5, bath application of the mGluR agonist, trans-ACPD (tACPD), is**
376 **known to increase astrocyte $[Ca^{2+}]_i$ in younger animals (Mulligan and MacVicar, 2004).**
377 Therefore, **tACPD** was used to evoke reliable, reproducible astrocyte $[Ca^{2+}]_i$ **elevations** in
378 acute brain slices **from juvenile rats.** In order to evoke widespread increases in astrocyte
379 $[Ca^{2+}]_i$, hippocampal-neocortical slices were perfused with trans-ACPD (tACPD), an mGluR
380 agonist. Application of tACPD (100μM) to brain slices (from juvenile rats) caused a
381 generalized increase in astrocyte $[Ca^{2+}]_i$, observed using 2PLSM (Figure 2A-C), that
382 provided us with the ability to measure subsequent synthesis of $PgE_2$. Applying tACPD
383 resulted in the formation and efflux of $PgE_2$, as measured by ELISA (Figure 2D). The first
384 step in the conversion of AA to $PgE_2$ in astrocytes is via COX-1 (Figure 7 and Takano et al.,
385 2006; Gordon et al., 2008; Font-Nieves et al., 2012). Neurons, in contrast, express COX-2
386 but not COX-1 (Nogawa et al., 1997). In support of a central role for COX-1, we found that,
387 although the tACPD-evoked increase in astrocyte $[Ca^{2+}]_i$ was unaltered (Figure 2C) in the
388 presence of the COX-1 inhibitor SC560 (Smith et al., 1998) (100nM: Blanco et al., 2008), the
389 resulting formation and efflux of $PgE_2$, as measured by ELISA, was abolished ($p<0.001$,
390 Figure 2D). Thus, astrocyte COX-1 activity is required for the subsequent $PgE_2$ release in
391 acute brain slices which is triggered by astrocyte $[Ca^{2+}]_i$ **signals**.

Downstream of COX-1, the synthesis of $PgE_2$ involves the enzyme mPgES-1 (Tachikawa et al., 2012), a form of prostaglandin E synthase expressed in astrocytes (Figure 3A and Tachikawa et al., 2012) that requires the co-factor GSH (Jakobsson et al., 1999; Murakami et al., 2000). It is known that GSH is present in high levels in astrocytes (Sun et al., 2006; Bragin et al., 2010; Robillard et al., 2011), as detected by staining of brain tissue with monochlorobimane (MCB), a GSH-sensitive dye (Figure 3B). Therefore we investigated whether $PgE_2$ formation was reduced when GSH levels were depressed. We examined whether there is a reduction in astrocyte $[Ca^{2+}]_i$-evoked $PgE_2$ release in hippocampal slices after treatment with buthionine sulfoximine (BSO, an inhibitor of γ-glutamylcysteine synthetase) for 2.5 hours (Sun et al., 2006), which reduced the tissue GSH concentration by 27% ($p = 0.009$, Figure 2E). When GSH levels were decreased, although there was no change in basal $PgE_2$ efflux (Figure 2D) or in the amplitude of tACPD-evoked astrocyte $[Ca^{2+}]_i$ **signals** (Figure 2A-C), strikingly the tACPD-evoked $PgE_2$ efflux was reduced by 64% ($p<0.001$, Figure 2D).

**Astrocyte $[Ca^{2+}]_i$ signals evoke COX-1 and GSH-dependent vasodilations in brain slices**

As COX-1 activity (Niwa et al., 2001) and $PgE_2$ release (Wagerle and Mishra, 1988; Wagerle and Degiulio, 1994) have been shown to lead to increased CBF in response to hypercapnia, we examined whether COX-1-dependent $PgE_2$ release evoked by astrocyte $[Ca^{2+}]_i$ **signals** triggered by either **tACPD application** or $IP_3$ uncaging resulted in vasodilations.

Bath perfusion of tACPD induced arteriolar dilation in acute brain slices (Figure 2A,F,G) which was abolished in the presence of SC560 ($p<0.01$, Figure 2G) while the amplitude of evoked astrocyte $[Ca^{2+}]_i$ **signals** was unchanged ($p>0.05$, Figure 2C). Thus, combined with the results discussed above, these data confirm that astrocyte COX-1 activity and subsequent

416 $PgE_2$ release are required for vasodilations in acute brain slices that are triggered by astrocyte
417 $[Ca^{2+}]_i$ **signals**.

418 As previously discussed, downstream of COX-1, the synthesis of $PgE_2$ involves the
419 astrocyte-expressed, GSH-dependent, enzyme mPgES-1 (Tachikawa et al., 2012). Therefore
420 a role for astrocytes in the regulation of arteriole diameter would be supported if $[Ca^{2+}]_i$-
421 evoked vasodilations were attenuated when GSH levels were depressed. We examined
422 whether there is a reduction in subsequent vasodilations in hippocampal slices after treatment
423 with BSO. When GSH levels were decreased, tACPD-evoked astrocyte $[Ca^{2+}]_i$ **signals** were
424 unaltered (Figure 2A-C). However, the vasodilations triggered by these $[Ca^{2+}]_i$ **signals** were
425 abolished (Figure 2A,F,G, $p<0.01$). Vasoconstrictions evoked by norepinephrine (NE,
426 100μM) or the $\alpha_2$ agonist clonidine (10μM), which act directly on arteriole smooth muscle
427 cells (Busija and Leffler, 1987), were unchanged in the presence of BSO (Figure 2A,G,H),
428 indicating that arterioles were not damaged by the BSO treatment. Furthermore, BSO
429 treatment did not alter the vasodilation evoked by either 1μM $PgE_2$ (Figure 2H) or high $[K^+]$
430 (10mM), which causes vasodilation by hyperpolarizing arteriole smooth muscle cells (Filosa
431 et al., 2006) ($K^+$: 8.6±2.3%, n=5 slices from 5 rats. BSO + $K^+$: 6.5±0.8%, n=6 slices from 3
432 rats, $p=0.37$).

433 Astrocyte $[Ca^{2+}]_i$ increases can be triggered by two-photon uncaging of $IP_3$ within the cell
434 body of an astrocyte. Using this technique, we directly examined the effect of decreasing
435 GSH levels on astrocyte $[Ca^{2+}]_i$-evoked arteriole dilations. Astrocytes in hippocampal slices
436 from juvenile rats were bulk-loaded with the caged $IP_3$ compound, NV-$IP_3$/AM. Two-photon
437 photolysis was used to uncage $IP_3$ within an astrocyte soma specifically, generating a $[Ca^{2+}]_i$
438 increase within the soma, processes and endfeet. This local increase in $[Ca^{2+}]_i$ could evoke an
439 increase in $[Ca^{2+}]_i$ in nearby astrocytes (Figure 4A,B, represents local and propagated

responses) and elicited vasodilation of the neighboring arteriole (Figure 4C). Although astrocyte $[Ca^{2+}]_i$ **signals** were unaltered following BSO treatment to reduce GSH levels (p=0.1, Figure 4A,B), dilations were not observed and vasoconstrictions were now evoked (p=0.008, Figure 4C). Thus, when GSH levels are reduced astrocyte $[Ca^{2+}]_i$ **signals** can no longer evoke vasodilations normally triggered by the release of $PgE_2$.

***In vivo* hypercapnia-evoked CBF responses are GSH dependent**

Having determined in acute brain slices the vasodilatory molecules underlying astrocyte $[Ca^{2+}]_i$-evoked vasodilations, we examined whether these same enzymes and molecules were involved in the CBF response which occurs downstream of $CO_2$-evoked astrocyte $[Ca^{2+}]_i$ responses *in vivo*. Hypercapnia *in vivo* evoked a CBF increase in the barrel cortex of adult rat (Figure 5A,B,D,E) while neural activity was unchanged (Figure 5F). The calculated area under the curve (AUC) of the CBF response was significantly attenuated by SC560 (p=0.032, Figure 5A,B), confirming that COX-1 plays a critical role in hypercapnia-evoked CBF increases *in vivo* (Niwa et al., 2001).

We examined the impact of decreased tissue GSH levels on $CO_2$-evoked CBF increases *in vivo*. To lower GSH levels *in vivo*, BSO was injected into rat barrel cortex. After 24 hours, tissue GSH levels in the ipsilateral cortex were reduced by 45% (Figure 5C, p=0.018). Treatment with BSO reduced the hypercapnia-evoked CBF response (Figure 5D,E, AUC reduced by 65%, p = 0.048). Neural activity was no different in BSO-treated rats compared to saline-treated rats (Figure 5G). Combining all the data described so far suggests that hypercapnia-evoked, astrocyte $[Ca^{2+}]_i$-related, CBF increases require $PgE_2$ release and, thus, are compromised when brain GSH levels are reduced.

This finding was specific to hypercapnia-evoked CBF increases. We examined the impact of decreased tissue GSH levels *in vivo* on functional hyperemia in the somatosensory

464 cortex. Whisker pad stimulation (10Hz) evoked a blood flow increase in the barrel cortex
465 (Figure 6A). In agreement with previous findings (Niwa et al., 2000), inhibiting COX-1 with
466 SC560 had no effect on either the CBF response to whisker pad stimulation (Figure 6A-B, p
467 = 0.10) or evoked neural activity (LFP, Figure 6C, p=0.91). Furthermore, the AUC of the
468 stimulation-evoked CBF response was not significantly different in BSO-treated animals
469 (Figure 6D, p = 0.14) compared to saline-treated animals, demonstrating that the CBF
470 response is not GSH-sensitive. The magnitude of the neural response to whisker pad
471 stimulation was unaffected by BSO (Figure 6E, p = 0.68). These results indicate that, under
472 these experimental conditions, COX-1 and GSH play little, if any, role in the CBF response
473 to somatosensory stimulation. These findings confirm that several different pathways exist
474 which account for CBF regulation under differing conditions and in response to different
475 stimuli.

476 **Discussion**

477 We demonstrate a novel mechanism of CBF regulation involving astrocytes, which is
478 GSH dependent. Previously, Niwa et al. (2001) demonstrated that hypercapnia-evoked CBF
479 increases are principally COX-1 dependent. In this study, we examined the mechanism of
480 such CBF regulation, both up- and downstream of hypercapnia-evoked increases in COX-1
481 activity (Figure 7). We demonstrate *in vivo* that, upstream of evoked COX-1 activity, $CO_2$
482 increases $[Ca^{2+}]_i$ in astrocytes. These data demonstrate a new signal (hypercapnia) that
483 activates astrocyte calcium and specifically identify the involvement of astrocytes in the
484 regulation of CBF in response to changes in arterial $CO_2$.

485 *In vitro*, using brain slices from juvenile animals in which it is possible to examine
486 calcium signals by bulk loading a calcium indicator dye, we confirm that increased astrocyte
487 $[Ca^{2+}]_i$ results in the subsequent release of $PgE_2$ and vasodilation which are COX-1 activity-

dependent (Figure 7). Our assumption that the evoked response in juvenile rat slices is the same as in adult rat with respect to COX-1 dependence is supported by the fact that the same COX-1 dependence has been shown in adult mice (Takano et al., 2006). We demonstrate that these findings hold *in vivo*, confirming previous findings in adult mice (Niwa et al., (2001)). Astrocytic endfeet, which are apposed to cerebral vascular smooth muscle, express all the machinery necessary for $PgE_2$ synthesis (COX-1: (Takano et al., 2006; Gordon et al., 2008), mPgES-1: (Figure 3A and Tachikawa et al., 2012), and GSH: (Figure 3B and Sun et al., 2006; Bragin et al., 2010; Robillard et al., 2011)), providing further evidence for the involvement of astrocytes in the regulation of CBF responses to hypercapnia. mPgES, an enzyme selectively expressed in astrocytes as compared to neurons (Tachikawa et al., 2012) is the enzyme responsible for producing $PgE_2$ downstream of COX-1 activity. Intriguingly the formation of $PgE_2$ is regulated by the availability of GSH in astrocytes, as PgES requires GSH as a co-factor (Jakobsson et al., 1999; Murakami et al., 2000). *In vitro,* we demonstrate that astrocyte $[Ca^{2+}]_i$-evoked vasodilations are attenuated when GSH levels are depleted, while *in vivo*, we demonstrate that $CO_2$-evoked CBF increases occur via a GSH dependent mechanism. As astrocytes contain high levels of GSH (Figure 3B and Sun et al., 2006; Bragin et al., 2010; Robillard et al., 2011), the dependence of the $CO_2$-evoked CBF response on GSH is further evidence of astrocytic involvement. Taken together, our findings suggest a novel mechanism of astrocyte-evoked CBF regulation which is GSH dependent. We propose that increased $CO_2$ levels evoke $[Ca^{2+}]_i$ responses in astrocytes, subsequently activating a signaling pathway, involving COX-1 and the GSH-dependent PgES, which results in the release of the vasodilator $PgE_2$. Thus, an increase in $CO_2$ results in an astrocyte-driven, GSH-dependent vasodilation (Figure 7).

511 This GSH-dependent mechanism of CBF regulation exists alongside other COX-1 and
512 GSH insensitive mechanisms. For example, we found no effect of blocking COX-1 activity
513 or of lowering GSH levels on CBF responses following **10Hz** whisker pad stimulation.
514 **While it is possible that an astrocyte calcium response (and, thus, a GSH-sensitive**
515 **mechanism of CBF regulation) may be evoked by an intense sensory stimulus (Schulz et**
516 **al., 2012; Sekiguchi et al., 2016), our results** are in agreement with previous work
517 suggesting that COX-1 is involved in CBF responses to hypercapnia (Niwa et al., 2001) but
518 not sensory stimulation (Niwa et al., 2000). While we saw no evidence that this pathway was
519 important for functional (neuronal activity-evoked) increases in CBF under our experimental
520 conditions, astrocytes appear to be an important intermediary for physiological (hypercapnia-
521 evoked) increases in CBF. Our findings suggest that CBF regulation may involve astrocytes,
522 and their $[Ca^{2+}]_i$ signals, under certain conditions and not under others.

523 Previous studies have provided evidence for several mechanisms linking astrocyte
524 $[Ca^{2+}]_i$, increases and changes in $CO_2$ concentration. For example**, within the respiratory**
525 **centre,** increased astrocyte $[Ca^{2+}]_i$, and astrocytic release of ATP, can be triggered by $CO_2$-
526 evoked decrease**s** in pH (Gourine et al., 2010). **This $[Ca^{2+}]_i$, increase may be the result of**
527 **increased $Na^+/HCO_3^-$ co-transport and reversal of $Na^+/Ca^{2+}$ transport (Turovsky et al.,**
528 **2016). It is unknown whether this mechanism also occurs within the cortex.**
529 Alternatively, increased $CO_2$ can evoke hemichannel-mediated release of ATP (Huckstepp et
530 al., 2010), which may act on astrocytic purinergic receptors to elicit an increase in $[Ca^{2+}]_i$
531 (Pelligrino et al., 2011). Depending on the mechanism linking increases in $CO_2$ to astrocyte
532 $[Ca^{2+}]_i$ responses, therefore, astrocytes could act as either a pH or $CO_2$ sensor. While it is
533 beyond the scope of this paper to determine the link between an increase in $CO_2$ and the
534 increase in astrocyte $[Ca^{2+}]_i$, we have demonstrated that the depletion of GSH levels leads to

535 a reduction in the ability of astrocytes to release $PgE_2$ following such a rise in $[Ca^{2+}]_i$, and so
536 reduces their ability to evoke vasodilation in response to hypercapnia. This occurs because
537 astrocytes express GSH dependent mPgES-1.

538 Our finding that CBF responses to increased $CO_2$ are GSH sensitive suggests that global
539 CBF regulation, which is sensitive to the partial pressure of arterial $CO_2$ (Ainslie and Duffin,
540 2009), will be affected in conditions where GSH levels are depleted. Alterations in the redox
541 status of brain tissue that are ultimately linked to cellular GSH levels have been observed in
542 numerous neurological and psychiatric disorders (Slivka and Cohen, 1993; Tohgi et al., 1995;
543 Tohgi et al., 1999; Ansari and Scheff, 2010; Zhang et al., 2012; Kulak et al., 2013).
544 Therefore, the impact of changes in GSH levels on the sensitivity of astrocyte regulation of
545 vasodilation could contribute to several CNS pathologies. Thus, it is critical to understand
546 the signaling pathways underlying changes in CBF, both in health and disease.

547 It has previously been shown that, in addition to astrocytic production of $PgE_2$ via COX-
548 1/mPgES activity, neurons (which express COX-2 but not COX-1 (Nogawa et al., 1997;
549 Lecrux et al., 2011)), are capable of producing COX-2-derived $PgE_2$ (which contributes to
550 neurovascular coupling: Lecrux et al., 2011; Lacroix et al., 2015). In this study, we used a
551 pharmacological approach **to increase astrocyte $[Ca^{2+}]_i$** and to inhibit either the *de novo*
552 synthesis of glutathione or the activity of COX-1, specifically, to demonstrate that
553 downstream of an increase in astrocyte $[Ca^{2+}]_i$, COX-1 activity and glutathione are required
554 for vasodilation to occur. However, as this pharmacological approach lacks cellular
555 specificity, a contribution of neuronally-produced $PgE_2$ to the hypercapnia-evoked CBF
556 response cannot be completely excluded. Nevertheless, our conclusion that astrocyte COX-1-
557 derived $PgE_2$, rather than neuronal COX-2-derived $PgE_2$, is involved in the CBF response to
558 hypercapnia is in agreement with previous findings (Niwa et al., 2001). Future studies could

559 use an astrocyte specific genetic strategy (such as cell-specific knockout: Casper et al., 2007)
560 to confirm that hypercapnia-evoked vasodilations, occurring downstream of astrocyte $[Ca^{2+}]_i$
561 responses, are dependent on astrocyte glutathione levels and COX-1 activity.

562 In conclusion, we demonstrate a novel mechanism by which astrocytes detect
563 hypercapnia and, via $[Ca^{2+}]_i$ signals, increase CBF in response to $CO_2$. Astrocytes are
564 therefore poised to detect the metabolic activity of neurons and to modify vascular tone
565 appropriately to deliver glucose and $O_2$. This important pathway may be impaired in
566 conditions in which oxidative stress reduces GSH levels in astrocytes, leading to impaired
567 CBF responses and altered vascular readouts of neural activity.

568

569 **References**


570 Ainslie PN, Duffin J (2009) Integration of cerebrovascular CO2 reactivity and chemoreflex
571 control of breathing: mechanisms of regulation, measurement, and interpretation.
572 American journal of physiology Regulatory, integrative and comparative physiology
573 296:R1473-1495.

574 Ansari MA, Scheff SW (2010) Oxidative stress in the progression of Alzheimer disease in the
575 frontal cortex. Journal of neuropathology and experimental neurology 69:155-167.

576 Attwell D, Buchan AM, Charpak S, Lauritzen M, Macvicar BA, Newman EA (2010) Glial
577 and neuronal control of brain blood flow. Nature 468:232-243.

578 Blanco VM, Stern JE, Filosa JA (2008) Tone-dependent vascular responses to astrocyte-
579 derived signals. American journal of physiology Heart and circulatory physiology
580 294:H2855-2863.

581 Bonder DE, McCarthy KD (2014) Astrocytic Gq-GPCR-Linked IP3R-Dependent Ca2+
582 Signaling Does Not Mediate Neurovascular Coupling in Mouse Visual Cortex In

583 Vivo. The Journal of neuroscience : the official journal of the Society for
584 Neuroscience 34:13139-13150.
585 Bragin DE, Zhou B, Ramamoorthy P, Muller WS, Connor JA, Shi H (2010) Differential
586 changes of glutathione levels in astrocytes and neurons in ischemic brains by two-
587 photon imaging. Journal of cerebral blood flow and metabolism : official journal of
588 the International Society of Cerebral Blood Flow and Metabolism 30:734-738.
589 Busija DW, Leffler CW (1987) Exogenous norepinephrine constricts cerebral arterioles via
590 alpha 2-adrenoceptors in newborn pigs. Journal of cerebral blood flow and
591 metabolism : official journal of the International Society of Cerebral Blood Flow and
592 Metabolism 7:184-188.
593 Cahoy JD, Emery B, Kaushal A, Foo LC, Zamanian JL, Christopherson KS, Xing Y,
594 Lubischer JL, Krieg PA, Krupenko SA, Thompson WJ, Barres BA (2008) A
595 transcriptome database for astrocytes, neurons, and oligodendrocytes: a new resource
596 for understanding brain development and function. J Neurosci 28:264-278.
597 Casper KB, Jones K, McCarthy KD (2007) Characterization of astrocyte-specific conditional
598 knockouts. Genesis 45:292-299.
599 Duffy S, MacVicar BA (1995) Adrenergic calcium signaling in astrocyte networks within the
600 hippocampal slice. The Journal of neuroscience : the official journal of the Society for
601 Neuroscience 15:5535-5550.
602 Filosa JA, Bonev AD, Straub SV, Meredith AL, Wilkerson MK, Aldrich RW, Nelson MT
603 (2006) Local potassium signaling couples neuronal activity to vasodilation in the
604 brain. Nature neuroscience 9:1397-1403.
605 Font-Nieves M, Sans-Fons MG, Gorina R, Bonfill-Teixidor E, Salas-Perdomo A, Marquez-
606 Kisinousky L, Santalucia T, Planas AM (2012) Induction of COX-2 enzyme and

down-regulation of COX-1 expression by lipopolysaccharide (LPS) control prostaglandin E2 production in astrocytes. J Biol Chem 287:6454-6468.

Gordon GR, Choi HB, Rungta RL, Ellis-Davies GC, MacVicar BA (2008) Brain metabolism dictates the polarity of astrocyte control over arterioles. Nature 456:745-749.

Gourine AV, Kasymov V, Marina N, Tang F, Figueiredo MF, Lane S, Teschemacher AG, Spyer KM, Deisseroth K, Kasparov S (2010) Astrocytes control breathing through pH-dependent release of ATP. Science 329:571-575.

Hauge A, Thoresen M, Walloe L (1980) Changes in cerebral blood flow during hyperventilation and CO2-breathing measured transcutaneously in humans by a bidirectional, pulsed, ultrasound Doppler blood velocitymeter. Acta physiologica Scandinavica 110:167-173.

He L, Linden DJ, Sapirstein A (2012) Astrocyte inositol triphosphate receptor type 2 and cytosolic phospholipase A2 alpha regulate arteriole responses in mouse neocortical brain slices. PLoS One 7:e42194.

Huckstepp RT, id Bihi R, Eason R, Spyer KM, Dicke N, Willecke K, Marina N, Gourine AV, Dale N (2010) Connexin hemichannel-mediated CO2-dependent release of ATP in the medulla oblongata contributes to central respiratory chemosensitivity. The Journal of physiology 588:3901-3920.

Jakobsson PJ, Thoren S, Morgenstern R, Samuelsson B (1999) Identification of human prostaglandin E synthase: a microsomal, glutathione-dependent, inducible enzyme, constituting a potential novel drug target. Proceedings of the National Academy of Sciences of the United States of America 96:7220-7225.

Kulak A, Steullet P, Cabungcal JH, Werge T, Ingason A, Cuenod M, Do KQ (2013) Redox dysregulation in the pathophysiology of schizophrenia and bipolar disorder: insights from animal models. Antioxidants & redox signaling 18:1428-1443.

632 Lacroix A, Toussay X, Anenberg E, Lecrux C, Ferreiros N, Karagiannis A, Plaisier F,
633 Chausson P, Jarlier F, Burgess SA, Hillman EM, Tegeder I, Murphy TH, Hamel E,
634 Cauli B (2015) COX-2-Derived Prostaglandin E2 Produced by Pyramidal Neurons
635 Contributes to Neurovascular Coupling in the Rodent Cerebral Cortex. The Journal of
636 neuroscience : the official journal of the Society for Neuroscience 35:11791-11810.
637 Lathia JD, Okun E, Tang SC, Griffioen K, Cheng A, Mughal MR, Laryea G, Selvaraj PK,
638 ffrench-Constant C, Magnus T, Arumugam TV, Mattson MP (2008) Toll-like receptor
639 3 is a negative regulator of embryonic neural progenitor cell proliferation. J Neurosci
640 28:13978-13984.
641 Lecrux C, Toussay X, Kocharyan A, Fernandes P, Neupane S, Levesque M, Plaisier F,
642 Shmuel A, Cauli B, Hamel E (2011) Pyramidal neurons are "neurogenic hubs" in the
643 neurovascular coupling response to whisker stimulation. The Journal of neuroscience
644 : the official journal of the Society for Neuroscience 31:9836-9847.
645 Lind BL, Brazhe AR, Jessen SB, Tan FC, Lauritzen MJ (2013) Rapid stimulus-evoked
646 astrocyte Ca2+ elevations and hemodynamic responses in mouse somatosensory
647 cortex in vivo. Proceedings of the National Academy of Sciences of the United States
648 of America 110:E4678-4687.
649 Mulligan SJ, MacVicar BA (2004) Calcium transients in astrocyte endfeet cause
650 cerebrovascular constrictions. Nature 431:195-199.
651 Murakami M, Naraba H, Tanioka T, Semmyo N, Nakatani Y, Kojima F, Ikeda T, Fueki M,
652 Ueno A, Oh S, Kudo I (2000) Regulation of prostaglandin E2 biosynthesis by
653 inducible membrane-associated prostaglandin E2 synthase that acts in concert with
654 cyclooxygenase-2. The Journal of biological chemistry 275:32783-32792.
655 Nimmerjahn A, Kirchhoff F, Kerr JN, Helmchen F (2004) Sulforhodamine 101 as a specific
656 marker of astroglia in the neocortex in vivo. Nat Methods 1:31-37.

Niwa K, Haensel C, Ross ME, Iadecola C (2001) Cyclooxygenase-1 participates in selected vasodilator responses of the cerebral circulation. Circ Res 88:600-608.

Niwa K, Araki E, Morham SG, Ross ME, Iadecola C (2000) Cyclooxygenase-2 contributes to functional hyperemia in whisker-barrel cortex. The Journal of neuroscience : the official journal of the Society for Neuroscience 20:763-770.

Nizar K et al. (2013) In vivo stimulus-induced vasodilation occurs without IP3 receptor activation and may precede astrocytic calcium increase. The Journal of neuroscience : the official journal of the Society for Neuroscience 33:8411-8422.

Nogawa S, Zhang F, Ross ME, Iadecola C (1997) Cyclo-oxygenase-2 gene expression in neurons contributes to ischemic brain damage. J Neurosci 17:2746-2755.

Olajide OA, Velagapudi R, Okorji UP, Sarker SD, Fiebich BL (2014) Picralima nitida seeds suppress PGE2 production by interfering with multiple signalling pathways in IL-1beta-stimulated SK-N-SH neuronal cells. J Ethnopharmacol 152:377-383.

Otsu Y, Couchman K, Lyons DG, Collot M, Agarwal A, Mallet JM, Pfrieger FW, Bergles DE, Charpak S (2015) Calcium dynamics in astrocyte processes during neurovascular coupling. Nature neuroscience 18:210-218.

Pelligrino DA, Vetri F, Xu HL (2011) Purinergic mechanisms in gliovascular coupling. Seminars in Cell & Developmental Biology 22:229-236.

Petzold GC, Albeanu DF, Sato TF, Murthy VN (2008) Coupling of neural activity to blood flow in olfactory glomeruli is mediated by astrocytic pathways. Neuron 58:897-910.

Pileblad E, Magnusson T (1989) Intracerebroventricular administration of L-buthionine sulfoximine: a method for depleting brain glutathione. J Neurochem 53:1878-1882.

Robillard JM, Gordon GR, Choi HB, Christie BR, MacVicar BA (2011) Glutathione restores the mechanism of synaptic plasticity in aged mice to that of the adult. PloS one 6:e20676.

682 Rosenegger DG, Tran CH, Wamsteeker Cusulin JI, Gordon GR (2015) Tonic Local Brain
683 Blood Flow Control by Astrocytes Independent of Phasic Neurovascular Coupling.
684 The Journal of neuroscience : the official journal of the Society for Neuroscience
685 35:13463-13474.
686 Schulz K, Stydekum E, Krueppel R, Engelbrecht CJ, Schlegel F, Schroter A, Rudin M,
687 Helmchen F (2012) Simultaneous BOLD fMRI and fiber-optic calcium recording in
688 rat neocortex. Nat Methods 9:597-602.
689 Sekiguchi KJ, Shekhtmeyster P, Merten K, Arena A, Cook D, Hoffman E, Ngo A,
690 Nimmerjahn A (2016) Imaging large-scale cellular activity in spinal cord of freely
691 behaving mice. Nat Commun 7:11450.
692 Slivka A, Cohen G (1993) Brain ischemia markedly elevates levels of the neurotoxic amino
693 acid, cysteine. Brain Res 608:33-37.
694 Smith CJ, Zhang Y, Koboldt CM, Muhammad J, Zweifel BS, Shaffer A, Talley JJ, Masferrer
695 JL, Seibert K, Isakson PC (1998) Pharmacological analysis of cyclooxygenase-1 in
696 inflammation. Proceedings of the National Academy of Sciences of the United States
697 of America 95:13313-13318.
698 Sun W, McConnell E, Pare JF, Xu Q, Chen M, Peng W, Lovatt D, Han X, Smith Y,
699 Nedergaard M (2013) Glutamate-dependent neuroglial calcium signaling differs
700 between young and adult brain. Science 339:197-200.
701 Sun X, Shih AY, Johannssen HC, Erb H, Li P, Murphy TH (2006) Two-photon imaging of
702 glutathione levels in intact brain indicates enhanced redox buffering in developing
703 neurons and cells at the cerebrospinal fluid and blood-brain interface. The Journal of
704 biological chemistry 281:17420-17431.

705 Tachikawa M, Ozeki G, Higuchi T, Akanuma S, Tsuji K, Hosoya K (2012) Role of the
706 blood-cerebrospinal fluid barrier transporter as a cerebral clearance system for
707 prostaglandin E(2) produced in the brain. J Neurochem 123:750-760.
708 Takano T, Tian GF, Peng W, Lou N, Libionka W, Han X, Nedergaard M (2006) Astrocyte-
709 mediated control of cerebral blood flow. Nature neuroscience 9:260-267.
710 Takata N, Nagai T, Ozawa K, Oe Y, Mikoshiba K, Hirase H (2013) Cerebral blood flow
711 modulation by Basal forebrain or whisker stimulation can occur independently of
712 large cytosolic Ca2+ signaling in astrocytes. PloS one 8:e66525.
713 Tanioka T, Nakatani Y, Semmyo N, Murakami M, Kudo I (2000) Molecular identification of
714 cytosolic prostaglandin E2 synthase that is functionally coupled with cyclooxygenase-
715 1 in immediate prostaglandin E2 biosynthesis. The Journal of biological chemistry
716 275:32775-32782.
717 Teng XW, Abu-Mellal AK, Davies NM (2003) Formulation dependent pharmacokinetics,
718 bioavailability and renal toxicity of a selective cyclooxygenase-1 inhibitor SC-560 in
719 the rat. J Pharm Pharm Sci 6:205-210.
720 Tohgi H, Abe T, Saheki M, Hamato F, Sasaki K, Takahashi S (1995) Reduced and oxidized
721 forms of glutathione and alpha-tocopherol in the cerebrospinal fluid of parkinsonian
722 patients: comparison between before and after L-dopa treatment. Neuroscience letters
723 184:21-24.
724 Tohgi H, Abe T, Yamazaki K, Murata T, Ishizaki E, Isobe C (1999) Increase in oxidized NO
725 products and reduction in oxidized glutathione in cerebrospinal fluid from patients
726 with sporadic form of amyotrophic lateral sclerosis. Neuroscience letters 260:204-
727 206.
728 Turovsky E, Theparambil S, Kasymov V, Deitmer J, Gutierrez del Arroyo A, Ackland G,
729 Corneveaux J, Allen A, Huentelman M, Kasparov S, Marina N, Gourine A (2016)

730 Mechanisms of $CO_2/H^+$ Sensitivity of Astrocytes. The Journal of Neuroscience
731 36:10750-10758.
732 Tuure L, Hamalainen M, Moilanen T, Moilanen E (2014) Aurothiomalate inhibits the
733 expression of mPGES-1 in primary human chondrocytes. Scand J Rheumatol:1-6.
734 Wagerle LC, Mishra OP (1988) Mechanism of CO2 response in cerebral arteries of the
735 newborn pig: role of phospholipase, cyclooxygenase, and lipoxygenase pathways.
736 Circ Res 62:1019-1026.
737 Wagerle LC, Degiulio PA (1994) Indomethacin-sensitive CO2 reactivity of cerebral
738 arterioles is restored by vasodilator prostaglandin. The American journal of
739 physiology 266:H1332-1338.
740 Zhang C, Rodriguez C, Spaulding J, Aw TY, Feng J (2012) Age-dependent and tissue-related
741 glutathione redox status in a mouse model of Alzheimer's disease. Journal of
742 Alzheimer's disease : JAD 28:655-666.
743 Zhang Y, Chen K, Sloan SA, Bennett ML, Scholze AR, O'Keeffe S, Phatnani HP, Guarnieri
744 P, Caneda C, Ruderisch N, Deng S, Liddelow SA, Zhang C, Daneman R, Maniatis T,
745 Barres BA, Wu JQ (2014) An RNA-sequencing transcriptome and splicing database
746 of glia, neurons, and vascular cells of the cerebral cortex. J Neurosci 34:11929-11947.
747 Zhang YH, Lu J, Elmquist JK, Saper CB (2003) Specific roles of cyclooxygenase-1 and
748 cyclooxygenase-2 in lipopolysaccharide-induced fever and Fos expression in rat
749 brain. J Comp Neurol 463:3-12.
750 Zonta M, Angulo MC, Gobbo S, Rosengarten B, Hossmann KA, Pozzan T, Carmignoto G
751 (2003) Neuron-to-astrocyte signaling is central to the dynamic control of brain
752 microcirculation. Nature neuroscience 6:43-50.

753 **Figure Legends**

**Figure 1: Astrocyte $[Ca^{2+}]_i$ transients are evoked by $CO_2$ *in vivo*.**

**A:** Example still images of mouse cortical layer II/III from 2PLSM. Oregon green bapta-1 (OGB) is used as a calcium indicator (i-iii) and sulforhodamine 101 (SR101, iv, average image for whole recording) is used to stain astrocytes. Colour scale refers to images i-iii. White arrows indicate astrocytes which show a $Ca^{2+}$ response to $CO_2$ of at least twice its baseline $Ca^{2+}$ fluctuation. In this case, $CO_2$ stimulus begins at t=0s and is applied for 36s. Image (iii) shows recovery of immediate $CO_2$ induced $Ca^{2+}$ transient. Scale bars 40µm. **B:** Further example images (i,iii) of mouse cortical layer II/III from 2PLSM showing example ROI placement. Merge images showing OGB and SR101 **(i, iii)**. Red ROI**1** indicates astrocyte **endfoot, red RO12 indicates astrocyte** soma (**layer II: n=181,** 8 mice), green ROI indicates neuron soma (**layer II: n=153,** 8 mice) and blue ROI indicates neuropil (**layer II: n=104,** 8 mice). Scale bar 20µm. Example time series (ii,iv) of $[Ca^{2+}]_i$ response in astrocyte **and neuron** soma ROI**s** (as indicated in i and iii). Blue box represents time during which expired $CO_2$ level is increased. **C:** Mean $Ca^{2+}$ response in ROIs, colours correspond to ROIs located as shown in **B** (i). **D:** Percentage of ROIs for each cell type which showed a $Ca^{2+}$ response with and without a hypercapnia stimulus. (For no hypercapnia (control), n=**170** astrocyte somas, n=**148** neuronal soma and n=**96** neuropil ROIs, n = 8 mice, colours correspond to description in **B**). **E:** Delay from hypercapnia start time to start of $Ca^{2+}$ response in ROI. **F:** Duration of $Ca^{2+}$ response in each ROI in response to $CO_2$ stimulus. Box plots shown in E,F show the mean (small square), edges of the box represent 25% and 75% of data and end lines represent maximum and minimum values. In all other panels, mean±s.e.m shown. ** $p < 0.01$, ***$p<0.001$.

**Figure 2: Astrocyte $[Ca^{2+}]_i$ signals evoke COX-1 and GSH dependent vasodilations *in vitro* .**

**A:** 2PLSM imaging: example $Ca^{2+}$ and arteriole diameter changes in response to tACPD with and without BSO. Images show overlay of pseudo-coloured $Ca^{2+}$ changes and transmitted light images. Dotted line indicates initial vessel diameter. Scale bar 10µm. **B:** Mean timecourse of increase in astrocyte $[Ca^{2+}]_i$ in response to tACPD. Coloured box indicates time of tACPD application. Control, n=56 from 26 rats, BSO, n=39 from 18 rats. **C:** Mean tACPD-evoked increase in astrocyte $[Ca^{2+}]_i$. tACPD, n=56 from 26 rats, tACPD + SC560, n=12 from 7 rats, tACPD + BSO, n=39 from 18 rats. **D:** Mean tACPD-evoked $PgE_2$ release, measured by ELISA. Within a group, each experiment (n) uses tissue from a different rat (i.e. control, n=8 from 8 rats). **E:** Mean tissue GSH concentration, data from 4 rats for each group. **F:** Mean time course of tACPD-evoked change in lumen diameter. Coloured box indicates time of tACPD application. Control, n=31 slices from 26 rats, BSO, n=21 slices from 18 rats. **G:** Mean changes in lumen diameter evoked by tACPD and clonidine. tACPD, n=31 slices from 26 rats, SC560+tACPD, n=7 slices from 7 rats, BSO+tACPD, n=21 slices from 18 rats, clonidine, n=8 slices from 8 rats, BSO+clonidine, n=8 slices from 7 rats. **H:** Mean changes in lumen diameter evoked by $PgE_2$ and norepinephrine (NE). $PgE_2$, n=5 slices from 4 rats, BSO+$PgE_2$, n=3 slices from 3 rats, NE, n=14 slices from 11 rats, BSO+NE, n=8 slices from 7 rats**.** Mean±s.e.m. shown. ** $p<0.01$, *** $p<0.001$. n is number of experiments conducted or, for calcium measurements, number of astrocyte ROIs analysed.

**Figure 3: Astrocytes express mPGES-1 and contain high levels of GSH.**

**A:** Immunohistochemistry showing astrocytic expression of GSH-dependent mPGES-1 in the CA3 of the hippocampus. Astrocyte marker, GFAP (red), mPGES-1 (green) and merge (yellow). Scale bar 20µm. **B:** Monochlorobimane (MCB) loaded hippocampal-neocortical slices. Astrocytes (identified by SR101, red, white arrowheads) contain higher levels of GSH

(as indicated by MCB staining, green) than neurons (white arrows). Merge (yellow). Scale bar 20μm.

**Figure 4: Astrocyte $[Ca^{2+}]_i$ transient-evoked vasodilations are GSH dependent *in vitro* .**

**A:** Mean $IP_3$-evoked increases in astrocyte $[Ca^{2+}]_i$. Control, n=21 from 6 rats, +BSO, n=11 from 4 rats. **B:** Mean timecourse of increase in astrocyte $[Ca^{2+}]_i$. Dotted line represents time of photolysis of caged $IP_3$. n as described in (**A**). **C:** Mean lumen diameter change in response to uncaging of $IP_3$. Uncage $IP_3$, n=11 slices from 6 rats, +BSO, n=6 slices from 4 rats. . Mean±s.e.m. shown. ** $p<0.01$. n is number of experiments conducted or, for calcium measurements, number of astrocyte ROIs analysed.

**Figure 5: $CO_2$ evoked CBF responses *in vivo* are GSH dependent.**

**A:** Mean traces of local CBF response to hypercapnia, measured by laser speckle contrast imaging, in vehicle (DMSO)- (blue) and SC560- (red) injected animals. n=7 rats for each group. Coloured box indicates time of $CO_2$ application. Data shown as fractional change with baseline of 0 (baseline taken during 60s pre-challenge) and a pre-treatment peak of 1 (shown as black dotted line on graph). **B:** Mean area under the curve (AUC) of CBF response to hypercapnia in the presence of vehicle (DMSO) or SC560 (normalized to pre-treatment maxima for each animal)**.** n=7 rats for each group. **C:** Tissue GSH levels 24 hours post-injection of BSO or saline into the barrel cortex (n=7 rats). **D:** Mean trace of local CBF response to hypercapnia, measured by laser Doppler flowmetry, in saline- (blue) and BSO- (red) injected rats. n=6 rats in each group. **E:** Mean values of AUC of CBF response to hypercapnia. n = 6 rats in each group. **F-G:** Neural activity: Power in frequency bands. **F:** During baseline (Base) and in response to hypercapnia (HCN) for saline- (blue) and BSO- (red) treated animals. n = 3 rats. **G:** Hypercapnia (HCN)/baseline (Base). Treatment with

BSO does not change the effect of hypercapnia on neural activity. n = 3 rats. Mean±s.e.m is shown. * $p < 0.05$.

**Figure 6: CBF responses to whisker pad stimulation *in vivo* are independent of GSH.**

**A:** Mean timecourse of local CBF response to whisker pad stimulation, measured by laser speckle contrast imaging, in vehicle (DMSO)- (blue) and SC560- (red) injected rats. Coloured box represents time of stimulation. Pre-treatment peak of 1 shown as dotted black line. **B:** Mean area under curve (AUC) of the CBF response to whisker pad stimulation, n=7 rats for each group. **C:** Mean neural response (LFP) magnitude to whisker pad stimulus (summed over total 16s length of stimulus). Responses are normalized to the first pulse response for each rat. n=4 DMSO-treated rats, n=3 SC560-treated rats. **D:** Mean AUC of the whisker pad stimulation-evoked CBF response in saline- (blue) and BSO- (red) injected rats, n=10 rats for each group. **E:** Mean neural response (LFP) magnitude to whisker pad stimulation (summed over total 16s length of stimulus). Responses are normalized to the first pulse response for each rat. n=3 rats in each group. Mean±s.e.m is shown.

**Figure 7: Increases in astrocytic $[Ca^{2+}]_i$ may lead to GSH-dependent, $PgE_2$-mediated vasodilation.**

Schematic diagram depicting how $CO_2$-evoked increases in astrocytic $[Ca^{2+}]_i$ may lead to $PgE_2$-mediated vasodilation. As a result of elevated $[Ca^{2+}]_i$, astrocytic phospholipase $A_2$ (PLA2) is activated. PLA2 generates arachidonic acid (AA) from the plasma membrane. AA can be processed locally by cyclooxygenase (COX) enzymes to produce AA derivatives such as prostaglandin $H_2$ ($PgH_2$). Prostaglandin $E_2$ ($PgE_2$) is produced from $PgH_2$ by the enzyme prostaglandin E synthase (PGEs) which requires glutathione (GSH) as a cofactor (Jakobsson et al., 1999; Murakami et al., 2000; Tanioka et al., 2000). $PgE_2$ is released from astrocyte

847 endfeet, which are apposed to the smooth muscle layer surrounding arterioles, resulting in
848 activation of $K^+$ channels, a decrease in $Ca^{2+}$ entry into the smooth muscle cell and
849 vasodilation.

850

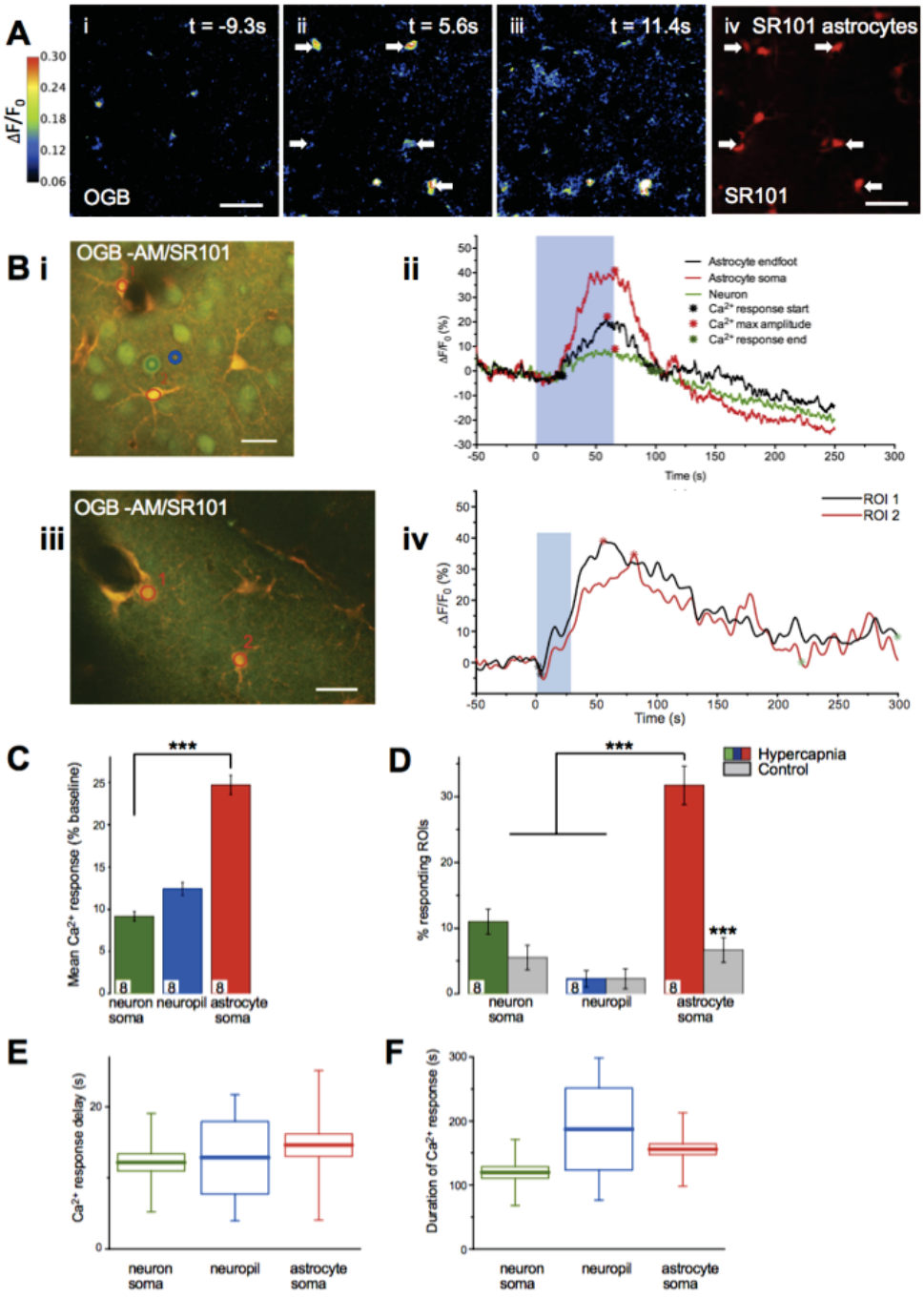
A
i
t = -9.3s
ii
t = 5.6s
iii
t = 11.4s
iv SR101 astrocytes
ΔF/F0
0.30
0.24
0.18
0.12
0.06
OGB
SR101
B i
OGB -AM/SR101
ii
Astrocyte endfoot
Astrocyte soma
Neuron
Ca2+ response start
Ca2+ max amplitude
Ca2+ response end
ΔF/F0 (%)
Time (s)
iii
OGB -AM/SR101
1
2
iv
ROI 1
ROI 2
ΔF/F0 (%)
Time (s)
C
***
Mean Ca2+ response (% baseline)
neuron soma
neuropil
astrocyte soma
D
***
Hypercapnia
Control
% responding ROIs
***
neuron soma
neuropil
astrocyte soma
E
Ca2+ response delay (s)
neuron soma
neuropil
astrocyte soma
F
Duration of Ca2+ response (s)
neuron soma
neuropil
astrocyte soma

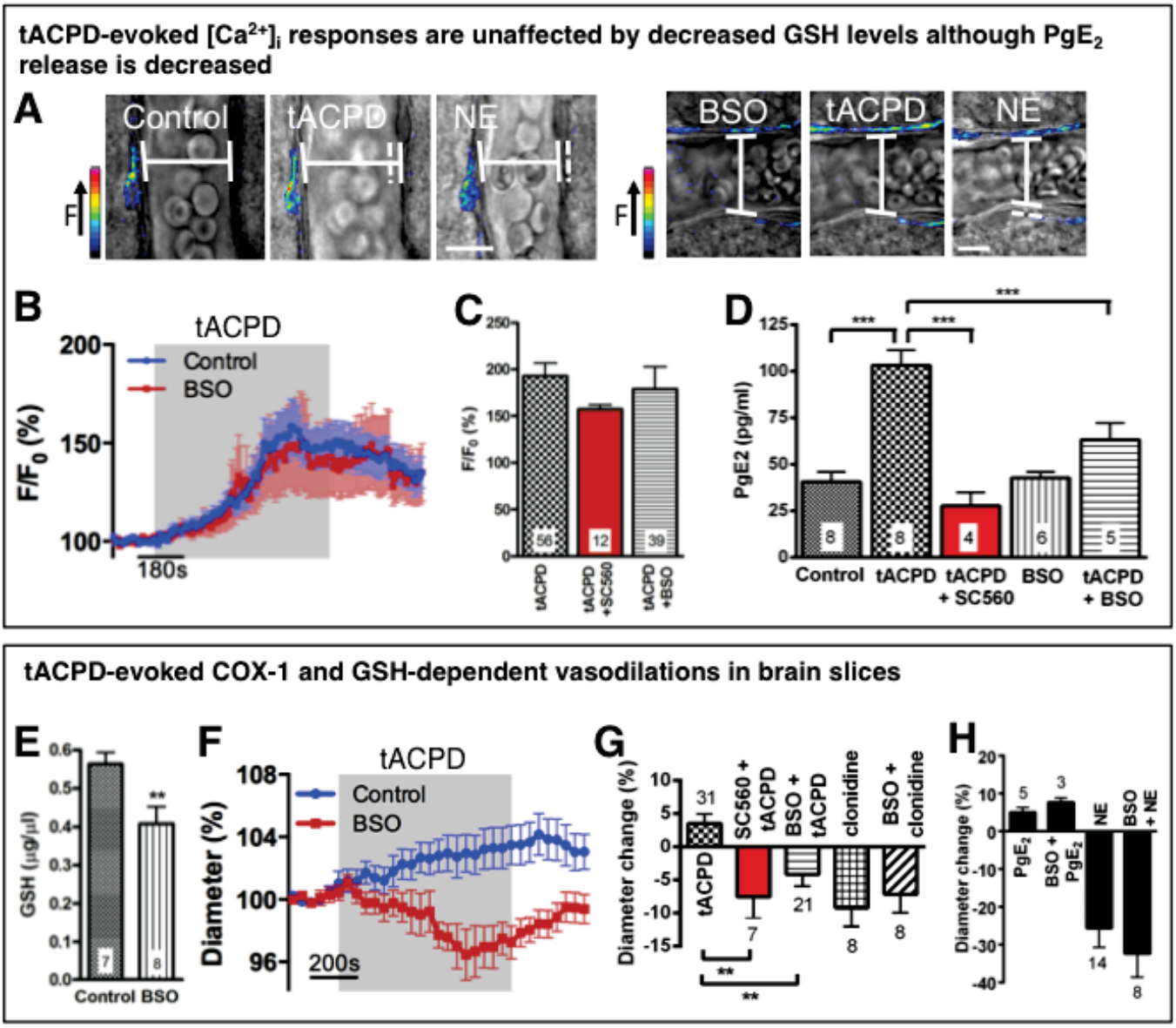
tACPD-evoked [Ca2+]i responses are unaffected by decreased GSH levels although PgE2 release is decreased
A
Control
tACPD
NE
BSO
tACPD
NE
F
B
tACPD
Control
BSO
F/F0 (%)
180s
C
F/F0 (%)
56
12
39
tACPD
tACPD +SC560
tACPD +BSO
D
PgE2 (pg/ml)
***
***
***
8
8
4
6
5
Control
tACPD
tACPD + SC560
BSO
tACPD + BSO
tACPD-evoked COX-1 and GSH-dependent vasodilations in brain slices
E
GSH (µg/µl)
**
7
8
Control
BSO
F
tACPD
Control
BSO
Diameter (%)
200s
G
Diameter change (%)
31
7
21
8
8
tACPD
SC560 + tACPD
BSO + tACPD
clonidine
BSO + clonidine
**
**
H
Diameter change (%)
5
3
14
8
PgE2
BSO + PgE2
NE
BSO + NE

**Figure 2**

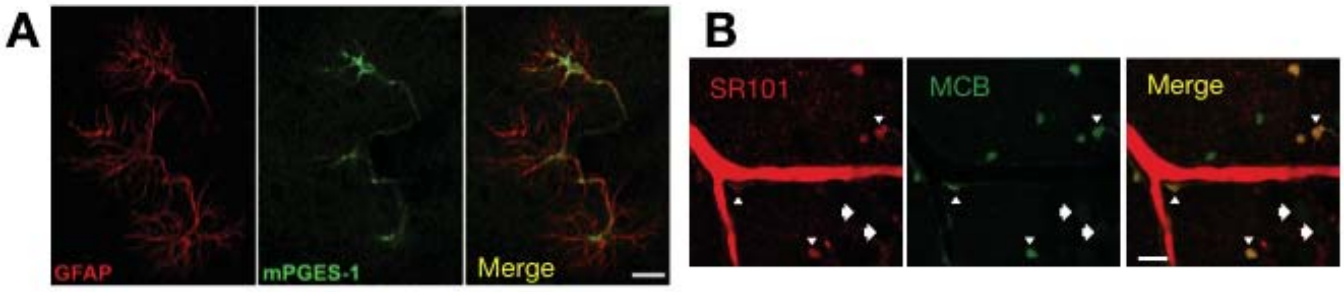


Figure 3

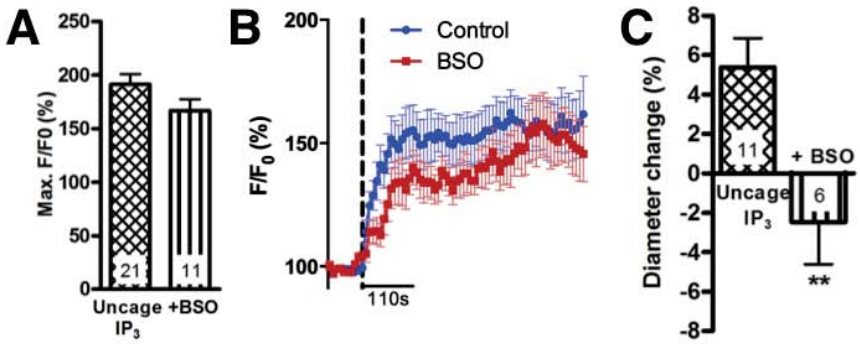
A
Max. F/F0 (%)
250
200
150
100
50
0
21
11
Uncage IP3
+BSO
B
F/F0 (%)
200
150
100
Control
BSO
110s
C
Diameter change (%)
8
6
4
2
0
-2
-4
-6
-8
11
Uncage IP3
+ BSO
6
**

**Figure 4**

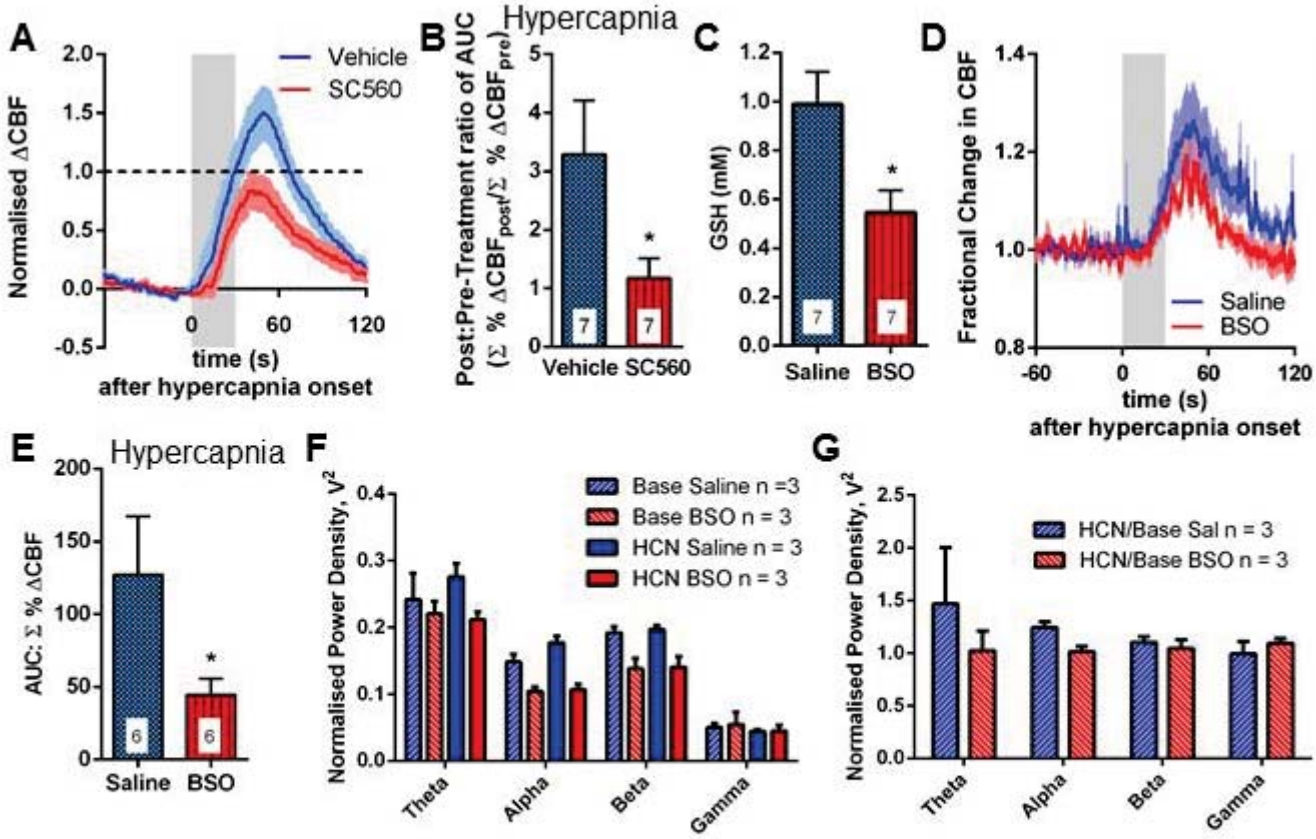
A
Normalised ΔCBF
Vehicle
SC560
time (s)
after hypercapnia onset
B
Hypercapnia
Post:Pre-Treatment ratio of AUC
(Σ % ΔCBFpost/Σ % ΔCBFpre)
Vehicle SC560
C
GSH (mM)
Saline BSO
D
Fractional Change in CBF
Saline
BSO
time (s)
after hypercapnia onset
E
Hypercapnia
AUC: Σ % ΔCBF
Saline BSO
F
Normalised Power Density, V²
Base Saline n =3
Base BSO n = 3
HCN Saline n = 3
HCN BSO n = 3
Theta
Alpha
Beta
Gamma
G
Normalised Power Density, V²
HCN/Base Sal n = 3
HCN/Base BSO n = 3
Theta
Alpha
Beta
Gamma

**Figure 5**

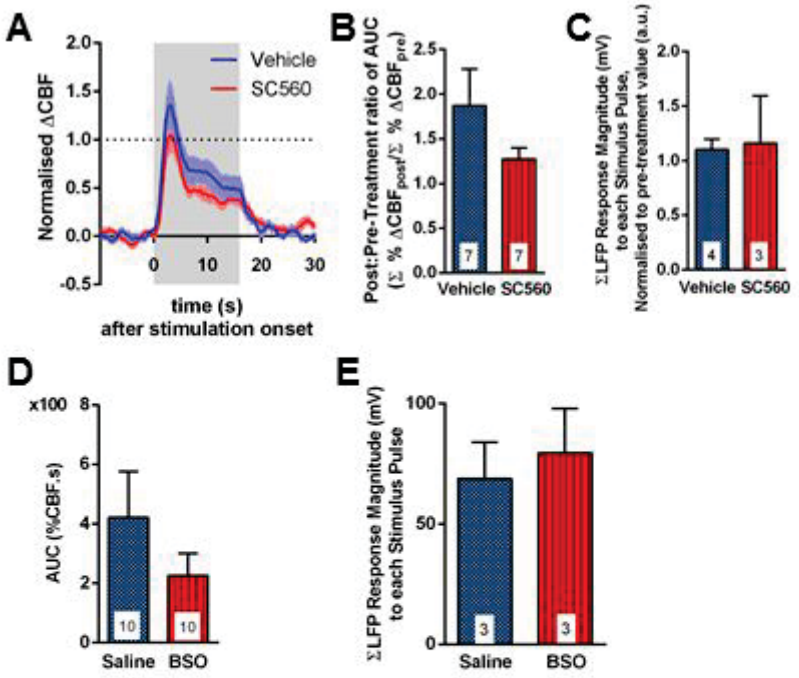
A
Normalised ΔCBF
Vehicle
SC560
time (s)
after stimulation onset
B
Post:Pre-Treatment ratio of AUC
(Σ % ΔCBF post/Σ % ΔCBF pre)
Vehicle SC560
C
ΣLFP Response Magnitude (mV)
to each Stimulus Pulse,
Normalised to pre-treatment value (a.u.)
Vehicle SC560
D
x100
AUC (%CBF.s)
Saline BSO
E
ΣLFP Response Magnitude (mV)
to each Stimulus Pulse
Saline BSO

**Figure 6**

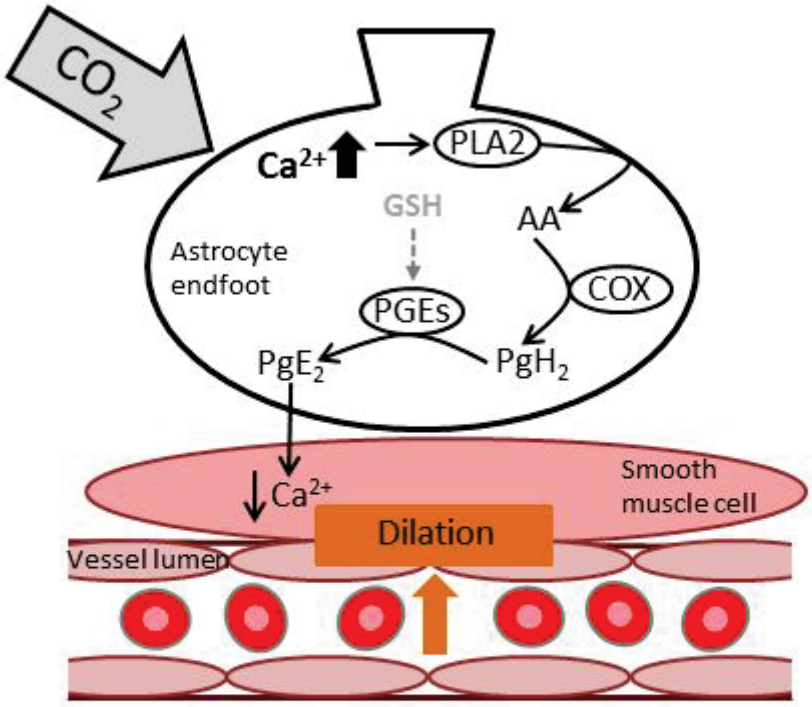
$CO_2$
$Ca^{2+}$
PLA2
GSH
AA
Astrocyte endfoot
COX
PGEs
$PgE_2$
$PgH_2$
$Ca^{2+}$
Smooth muscle cell
Dilation
Vessel lumen

**Figure 7**

**Table 1. Blood gases for BSO experiment (N.B. blood gases taken 24hrs post-drug but prior to hypercapnia and whisker stimulation experiments). Data presented as mean (SEM).**

| Treatment | pH | $pCO_2$ (mmHg) | $pO_2$ (mmHg) |
|---|---|---|---|
| Saline | 7.47 (0.01) | 34.5 (2.3) | 161 (4) |
| BSO* | 7.46 (0.01) | 35.8 (1.5) | 154 (7) |

* Buthionine sulfoximine (BSO, an inhibitor of γ-glutamylcysteine synthetase)

**Table 2. Blood gases for SC560 i.v. experiment (N.B. blood gases taken prior to and after drug administration). Data presented as mean (SEM).**

| Condition | Treatment | pH | $pCO_2$ (mmHg) | $pO_2$ (mmHg) |
|---|---|---|---|---|
| Pre-drug | DMSO | 7.47 (0.01) | 33.5 (1.5) | 164 (5) |
| | SC560 | 7.45 (0.01) | 36.8 (1.2) | 140 (5) |
| Post-drug | DMSO | 7.46 (0.01) | 34.1 (0.6) | 156 (6) |
| | SC560 | 7.45 (0.03) | 37.1 (2.1) | 140 (5) |